An efficient multi-scale approach for viscoelastic analysis of woven composites under bending

Vu An Le[a,b], Sanjay Nimbalkar[a], Navid Zobeiry[c], Sardar Malek[d,*]

[a] School of Civil and Environmental Engineering, University of Technology Sydney, 81 Broadway Street, Ultimo NSW 2007, Australia

[b] Department of Civil Engineering, The University of Danang, University of Science and Technology, 54 Nguyen Luong Bang Street, Da Nang, Vietnam

[c] Department of Materials Science and Engineering, University of Washington, Seattle, WA 98195, United States

[d] Department of Civil Engineering, University of Victoria, 3800 Finnerty Rd, Victoria, BC V8P 5C2, Canada

[*] Corresponding author, smalek@uvic.ca

Abstract

This paper investigates the bending response of cured and uncured viscoelastic composite laminates at different loading rates to gain a better understanding of the fibre waviness and wrinkling evolution during the forming process of advanced composites. This is accomplished by the implementation of a three-dimensional (3D) multi-scale modelling framework that incorporates analyses at different scales (micro-, meso- and macro-scale). For micro- and meso-scale simulations, analytical models proposed in the literature are investigated for estimating the material properties, while a differential form (DF) of viscoelasticity implemented as a UMAT is employed for structural level (macro-scale) simulations. Combining analytical equations at smaller scales with the DF form of viscoelasticity at macro-scale, a rapid method for estimating the effect of various parameters on wrinkle formation is developed. The numerical model is validated by comparing the bending behaviour of thin viscoelastic composites with experimental data reported in the literature. The influence of various parameters including fibre stiffness, ply anisotropy, resin properties, and loading rates on the bending behaviour of composites are analysed. The agreement between the numerical predictions and the experimental data highlights the potential of the proposed multi-scale modelling framework to predict the behaviour of viscoelastic composite with a variety of yarn architectures efficiently. Further experimental investigations into the viscoelastic characteristics of woven composites at the micro- and meso-scale are advised to ascertain the limitations and validity range of the predictions.

Keywords: Finite element analysis, bending, composites, viscoelastic materials, multi-scale, orthotropic properties, resin.

1. Introduction

Advanced composites are increasingly used for structural applications in aerospace, automotive, and marine industries thanks to their unique characteristics such as higher specific stiffness and strength, as well as ability for net shape manufacturing [1]. Woven-reinforced composites are preferred due to their improved ability to produce complex shapes [2]. However, formation of process-induced defects such as wrinkles poses obstacles to fully exploiting the potential of advanced composites [3]. Typically, aerospace industry process specifications limit the degree of defects for certification purposes. For instance, when it comes to wrinkles, the length and out-of-plane height of the wrinkles are kept within well-defined limits to minimise their influence on the mechanical performance of the end-part. Wrinkle development is facilitated during the forming process of complex composite components such as stringers by out-of-plane bending as well as in-plane shear deformations [4, 5]. As such, accurate prediction of in-plane and out-of-plane characteristics of an uncured laminate, as well as inter-ply slippage [6] during the forming process is highly desirable to optimize the forming process of composites and mitigate wrinkle formation. Although several studies on the bending properties of cured prepreg materials have been published, efficient numerical modelling of large viscoelastic composites remains a significant challenge in the composite manufacturing industry. Given that the high-fidelity simulation of viscoelastic behaviour of large composite parts during forming process takes significant set-up and computational time, industry often relies on trial-and-error experimental methods instead of simulation. This highlights the need for developing efficient simulation methods. This paper focuses on predicting the bending behaviour of woven composites using an efficient multi-scale modelling approach as a first step towards developing a fast and comprehensive multi-scale framework for viscoelastic analysis of woven composites during cure.

As the macro-scale mechanical properties of composites are closely linked to their microstructures, multi-scale modelling is an effective way to account for microstructural features on the macro-structural response of composites with complex microstructures [7-10]. Numerous frameworks for modelling of heterogeneous materials have been proposed over the years [11]. Based on the underlying problem formulation, modelling approaches can be classified into three categories; (i) concurrent, (ii) hierarchical and (iii) hybrid. Among these, the hierarchical modelling approach appears to be the most practical approach for industry applications and is thus considered in this paper. This approach entails describing different scales and employing techniques for resolving and coupling such hierarchical scales within a single domain.

At the macro or structural scale, the fundamental assumption in classical multi-scale modelling is that the material is homogeneous. The effective characteristics at the macro-scale are estimated by evaluating the micro-scale behaviour of a small representative volume element (RVE) of material across the macro domain [9]. As multiple analyses across different length scales are performed, using multi-scale methods significantly faster run times are obtained with minimal loss of accuracy compared to high-fidelity simulation approaches. Efficiency becomes critical in applications where the time-dependent (viscoelastic) response of the structure is of interest, such as in process modelling. In this context, Malek [12] proposed an efficient multi-scale approach for the analysis of composites with complex microstructures. The approach enables 3-D viscoelastic analysis of large-scale composite components with generally orthotropic properties. It should be noted that complex deformation mechanisms such as tow shear, inter-tow shear, inter-tow slip [5] were ignored to expedite the finite element analysis of uncured composites. Within this context, instead of explicitly considering complex mechanisms that may occur concurrently during the formation of woven composites, a modified input value at the micro-scale based on published experiments [6, 13-15] may be considered for uncured prepregs.

Bending properties of uncured thin laminates are known to significantly influence the occurrence of wrinkles, particularly in determining the shape of wrinkles [6, 16-18]. For example, increasing the bending rigidity of the laminate leads to an increase in the size of the wrinkles [19]. Numerous experimental studies [17, 20-23] have been conducted in the recent decade to characterise the out-of-plane bending behaviour of prepregs. To eliminate time-consuming and costly measurement trials, various researchers have developed numerical models for the composite forming process. Forming simulations for composite fabrics were carried out under the membrane hypothesis [14, 24], i.e., neglecting the bending stiffness. For example, Larberg and Åkermo [14] developed a methodology for modelling the in-plane deformations of unidirectional (UD) prepregs. Both in-plane shear and inter-ply friction were considered in the forming model of stacked thermoset UD prepregs in [14]. Subsequently, it was shown that bending stiffness has a substantial influence in determining the magnitude and intensity of wrinkles [16]. Other studies [6, 25, 26] suggested that the final desired shapes after forming of composite prepregs are determined by the complex interaction of intra-ply shear (including longitudinal and transverse intra-ply shearing), inter-ply slippage and out-of-plane bending. Numerous efforts have been made to incorporate such diverse deformation mechanisms into the composite forming model to accurately predict wrinkle evolution during the forming process. To capture such complex mechanisms, some researchers [6, 13, 27] have employed Aniform Finite Element (FE) software with shell elements to model the viscoelastic bending behaviour of composite plies under conditions relevant to the forming process. It is worth noting that the Aniform shell is a combination of a membrane element (LTR3D) and a Discrete Kirchhoff Triangle (DKT) element, which potentially can capture both in- and out-of-plane properties. However, time-consuming characterisation tests are required to determine the material parameters for a suitable constitutive model. For instance, the bias extension test was conducted and simulated in Aniform in order to obtain the fitted parameters for the membrane elements [1, 6]. Furthermore, despite the fact that a plate or shell theory can provide kinematics for points in the thickness, kinematics in the thickness of textile reinforcements is very specific, especially for thick textile reinforcements, due to relative slippage [16].

Accuracy of 3-D predictive tools highly depends on the input properties. For a reliable forming simulation, the properties of the uncured material must be accurately represented in the finite element models. As a result, significant research has concentrated on characterizing three types of rigidity that can be used as inputs to wrinkling simulations: tensile, in-plane shear, and bending [5, 13, 15, 19]. For this purpose, mechanical tests such as biaxial tests for tensile stiffness, picture-frame and bias-extension tests for in-plane shear stiffness and bending tests have been performed. The bias-extension test, which is a substitute for the picture-frame test, is intended to introduce pure shear into the material. As the in-plane shear behaviour is considered to be the most dominant deformation mechanism during forming process, finite element models have been developed using material models calibrated with bias-extension tests for in-plane shear stiffness [6, 13-15, 28]. Thereafter, the calibrated fibre stiffness values of uncured composites are retrieved from the measured shear data and used as inputs to the corresponding FE simulations of the bias extension tests. These fitted values for bias-extension simulations on specific composite prepregs available in the literature are summarized in Table 1. While Larberg and Åkermo [14] conducted bias-extension tests on cross-plied UD thermoset prepregs (T700/M21 and HTS/977-2), Haanappel et al. [15] applied bias-extension experiments for a woven glass fibre reinforcement (8HS/PPS). Bias-extension testing on multi-layer stack UD prepreg materials containing either HT (High Tenacity) fibre or IM (Intermediate Modulus) fibre and same matrix was considered by Sjölander et al. [28]. In recent studies conducted by [6, 13], using such a bias-extension test, the in-plane shear properties at forming conditions for 5HS satin weave impregnated with Cycom 5320 were characterized over a range of processing temperatures. The bias-extension response and simulation fit lead to a prediction of fibre stiffness as shown in Table 1. However, it should be noted that the value of the fibre stiffness was reduced compared to the real value reported in the data sheets to obtain a more stable simulation without a comprehensive investigation [13, 14, 28].

Bending tests have been widely used in the literature to assess ply bending stiffness for out-of-plane behaviour. Unlike cured composites, uncured prepregs may simultaneously promote mechanisms such as intra-ply slippages between fibres and local micro-buckling of fibres during bending since the resin is not stiff enough to prevent their occurrence [16, 18]. The combined deformations result in the composite prepregs having an apparent lower bending rigidity than conventional solid materials. Therefore, the bending properties have been investigated experimentally and characterized separately from the in-plane properties (tensile and compressive moduli) by [6, 28]. [6, 28] carried out cantilever bending tests and later calibrated the bending properties of a single ply using replication of the bending simulations. While Sjölander et al. [28] used an orthotropic elastic model to simulate the bending stiffness in the fibre direction and transverse to the fibre direction, Alshahrani and Hojjati [6] employed an isotropic viscoelastic material model for the out-of-plane bending elements. Table 1 lists the input parameters for the out-of-plane material properties based on the cantilever bending experiments. Similarly, Belnoue et al. [18] adapted the cantilever test proposed by Liang et al. [17] for capturing bending behaviour of a thermoplastic based prepreg at different temperatures. By measuring the bending stiffness in the fibre direction of an uncured prepreg ply (IMA-M21), material characteristic (i.e. Young's modulus along the fibre direction) was derived from the beam theory (see Table 1) and used as an input for the FE consolidation model. Dörr et al. [29], on the other hand, used a dynamic rheometer within a thermal chamber, rather than the more typically used static cantilever, to characterize the bending properties of a single ply of unidirectional (UD) reinforced PA6-CF tape. A constant parameter was used for the spring element in the viscoelastic material model to fit the bending characterization curve.

As discussed previously, the bending properties of an uncured prepreg were modelled separately from its in-plane properties using specific material models for the fibre and matrix [28, 30]. However, other researchers [31, 32] have attempted to relate bending stiffness to axial moduli (i.e. compressive and tensile modulus) using a hybrid model. Contrary to traditional isotropic materials, it is hypothesised that fibrous materials can exhibit significantly varied responses in tension and compression [31]. While fibre is extremely strong and stiff under tension, it will buckle with extremely modest compressive stresses. As a result, the bending stiffness of fibrous materials cannot be obtained directly from the tensile modulus; it must be measured through experiments [33]. For instance, the vertical cantilever method was used to analyse the bending behaviour of a cross-ply thermoplastic lamina, Dyneema HB80 (Ultra-High Molecular Weight Polyethylene fibres embedded in a polyurethane matrix [34], at elevated temperature (up to 120^{o}C). A tensile test was also conducted to measure the apparent elastic modulus of such thermoplastic composites as a function of temperature. Subsequently, the obtained tensile modulus and bending stiffness were used to calculate an effective compressive modulus following an equation proposed by Dangora et al. [31] for implementation into the finite element model. Similarly, Yu et al. [32] introduced an asymmetric axial modulus to calculate bending rigidity from the in-plane stiffness (i.e. tensile and compressive rigidities). The asymmetric axial modulus, defined as the ratio of compressive modulus to tensile modulus, was determined by conducting a cantilever deflection test in the warp and weft directions and then implemented into the FE software through a user material subroutine (Abaqus UMAT) for simulation of three-dimensional bending deformation. Alshahrani and Hojjati [26] derived an expression for the equivalent bending stiffness as a function of compressive, tensile and relaxation modulus. The compressive modulus of prepreg was determined by the slope of the stress-strain curve of an elastic region in a buckling test, while the tensile modulus was provided by the supplier. A generalized Maxwell model was used to fit the stress-relaxation response measured from the cantilever bending test, and parameters for the relaxation modulus were consequently obtained. The computed in-plane properties of the prepreg samples used as input parameters for FE bending models are listed in Table 1.

Considering experimental studies on uncured composites, it is apparent that accurate prediction of the mechanical properties of composites under bending is quite challenging. According to the extensive literature review conducted in this paper, it was found that regardless of the fibre type (i.e. carbon or glass fibre), fabric architecture (i.e. UD or woven fabrics) or impregnated resin, a low value of around 1 GPa, downscaled from a real value for the fibre stiffness (e.g., 200 GPa for carbon fibre), is commonly used in most numerical models [6, 13-15]. However, this low value has not been justified clearly in the literature [28]. Moreover, bending properties at elevated temperatures were estimated based on an educated guess [15]. Hence, a better understanding of the mechanical properties of uncured composites under bending is crucial for successful forming simulations. This is accomplished using a multi-scale modelling framework that incorporates analyses at different scales and is implemented in a general-purpose finite element code, Abaqus. Due to the limitation of Abaqus built-in viscoelastic model to isotropic materials, an orthotropic viscoelastic constitutive model implemented as a UMAT [12, 35] is considered. Using this material model, the influence of ply anisotropy on the bending behaviour is investigated.

It should be emphasized that the approach presented in this paper is a combination of closed-form equations and DF of viscoelastic behaviour. In comparison to other multi-scale approaches, this results in a much faster analysis. The complex deformation mechanisms that may occur simultaneously during bending of uncured composite prepregs are considered implicitly using a low value for fibre stiffness. Section 2 introduces the methodology for simulating the bending behaviour of prepregs using the DF of viscoelasticity. The details of the FE model and its verification are provided in Section 2. In Section 3, numerical results are compared with the experimental data available in the literature for validation purposes. The capabilities and limitations of the developed model are discussed in Section 4. Future works and conclusions are presented in Section 5.

2. Methodology

The viscoelastic behaviour of cantilever plates subjected to tip displacements can be modelled using the multi-scale approach introduced in [12] for orthotropic composites, as schematically shown in Fig. 1. It should be noted that similar approaches for analysing the response of complex 3D composites have been employed by other researchers (e.g. see [8, 9]). In this study, at lower scales (i.e., micro and meso) analytical models including micromechanics equations developed by Malek [12] and Naik [2] are used to predict the effective mechanical properties of a representing unit cell (RUC) of the woven fabric. These properties are then used as inputs for structural analysis at the macro-scale. The following sections describe the methodology in details.

2.1. Micro- and meso-scale analyses

At the micro-scale, the analytical micromechanics equations described in [12] are used to predict the effective viscoelastic properties of a representative volume element (RVE) of the solid unidirectional circular fibre composites with a specific fibre volume fraction (V_f) (see Fig. 1a). The effective properties obtained from the analytical homogenization at this scale is then used to estimate the properties of the fabric at the meso-scale. The fabric is composed of two sets of interlacing, mutually orthogonal (warp and weft) yarns. The selected weave type in this study is a 5-harness satin (see Fig. 1), which has advantages over plain and twill weaves in terms of drapability and conformity over complex shapes [23]. The periodicity of the repeating pattern in the woven fabric can be used to isolate a small repeating unit cell (RUC) which is sufficient to describe the fabric architecture. Details of meso-scale modelling of 5-harness satin weave composite and calculation of 3-D effective properties were described in [2]. The analytical procedure described in [2] was implemented in MATLAB for this study. Once the homogenized material properties at the meso-scale are estimated, they are employed directly as input properties for structural analysis at the macro-scale.

2.2. Macro-scale analysis

While the woven fabrics are discrete on the micro-scale, woven composites are assumed to be uniform and continuous at the macro-scale to simplify computations and improve the efficiency of the analysis. The macro-scale analysis of woven fabrics is mainly conducted to simulate the overall bending behaviour of the fabric using the micro- and meso-scale input parameters. To gain a deeper understanding of the deformation mechanisms, an analytical method is employed as an alternative to the numerical method in the macro-scale analysis. The analytical method at the macro-scale involves simple mathematical equations for predicting the deflection curve and moment vs curvature relation of an isotropic "elastic beam" under a small displacement. The numerical (finite element) method is then used to predict the bending moment-curvature relation of both "elastic" and "viscoelastic" composite plates at various loading rates.

For the viscoelastic analysis, the composite plate is first assumed to behave as a viscoelastic isotropic solid and modelled using the Abaqus built-in viscoelastic constitutive model which is based on the integral form (IF) of viscoelasticity. As the application of Abaqus viscoelastic model is limited to isotropic materials, a more versatile orthotropic viscoelastic constitutive model (based on a differential form of viscoelasticity – DF) that has been developed and implemented as a UMAT [12, 35] is then employed to elucidate the effect of ply anisotropy on the bending response of uncured 5-harness satin weave plates.

2.2.1. Analytical method

To estimate the bending behaviour of isotropic plates, simple mathematical equations for calculating the deflection of isotropic elastic beams are considered first. The beam dimensions and loads are selected based on the bending test conducted in [23]. The beam with dimensions of 10 mm in width, 0.55 mm in thickness and 150 mm in length has an overhang and therefore may be treated as a cantilever beam subjected to a load F acting at the free end (see Fig. 2a). The y and z-axis are defined as the distance along the axis of the undeformed beam and the vertical deflection of the beam, respectively (see Fig. 2b). For linearly elastic materials, moment-curvature relationship may be determined from the condition that the moment resultant of the bending stresses is equal to the bending moment M acting at the cross-section [36] as given by:

$$\kappa = \frac{1}{\rho} = \frac{M}{EI} \tag{1}$$

in which κ is the curvature, ρ is the radius of curvature of the deformed shape and EI is the flexural rigidity of the beam. It should be noted that an additional deflection term due to the shear deformation in the form of a mutual sliding of adjacent cross-sections along each other may be considered [37]. However, because of the very thin section of the cantilever beam (see Fig. 2a), the contribution of shear deformation is negligible compared to the bending of plies based on a detailed numerical simulation. For this purpose, a separate FE analysis was conducted on plies bonded with very soft interfaces to capture sliding of adjacent plies. Results suggested that the effect of shear deformation is less than 0.5% for the dimensions of the selected beam. In other words, bending has shown to be the dominating deformation mechanism in this test.

The exact expression for the curvature at any point along the curve is given by

$$\kappa = \frac{1}{\rho} = \frac{\frac{d^2z}{dy^2}}{\left[1+(\frac{dz}{dy})^2\right]^{3/2}} \tag{2}$$

According to Fig. 2a, the bending moment at a cross-section distance y from the fixed support is $M = FL - F(y)$. Since we are limiting to the elastic deformation and assuming that the slope of the elastic beam is small, the deflection curve of the beam can be derived as

$$z(y) = \frac{Fy^2}{EI}(\frac{L}{2} - \frac{y}{6}) \tag{3}$$

in which L is the length of the cantilever beam. Assuming that the cantilever beam AB subjected to a tip displacement of 10 mm (δ_B = 10 mm) (see Fig. 2b), the force required to achieve this displacement can be obtained as

$$F = \frac{3EI\delta_B}{L^3} \tag{4}$$

Finally, the moments at each point can be plotted against the corresponding curvature values.

2.2.2. Numerical method

Based on the review of bending modulus of uncured prepreg samples shown in Table 1, the cantilever beam is roughly assumed to be linearly isotropic elastic with Young' modulus and Poisson's ratio equal to 500 MPa and 0.2, respectively. It was restrained from all displacements in a length of 30 mm as it was gripped along this distance [23]. The beam was modelled in Abaqus using 20-noded solid quadratic brick element with reduced integration (C3D20R). Number of elements in width, length and thickness directions are 6, 50 and 2 respectively. Based on the convergence study similar to the one conducted in [38], the 1.67 mm × 2 mm × 0.275 mm mesh was selected and maintained uniformly for the whole beam.

Because Euler-Bernoulli beam theory is limited to small displacements, the free end of the cantilever beam is displaced by 10 mm. Indeed, the maximum deflection (δ_B = 10 mm) (see Fig. 2b) is less than 10 % of the free span length (120 mm) which meets the requirement of a small deformation problem. It is also noted that the loading point is 4 mm from the free end of the beam as suggested in [23]. The load value required to achieve a certain tip displacement noted in the experiment is used to calculate the bending moment along the length of the beam. Through capturing the bending curve corresponding to the maximum displacement reached (see Fig. 3a), deflection profile $z(y)$ is fitted using a proper polynomial function. The expression for the curvature is subsequently calculated as an equation of the second derivative of z with respect to y according to Euler-Bernoulli's law for small deformation.

Using Euler-Bernoulli beam theory, the equation of the deflection curve for a bending beam AB (Fig. 2a) subjected to a concentrated load F at point B can be determined by using Eq. (3) With the known value of the corresponding displacement at point B, the unknown load F can easily be calculated using Eq. (4). Finally, the obtained bending moment along the length of the beam can be plotted against the corresponding curvature of the beam (Fig. 3b). The agreement between results from the present finite element analysis with the theoretical prediction both in bending profile (Fig. 3a) and moment – curvature plot (Fig. 3b) verifies the FE model in term of mesh size, applied load and boundary conditions.

The above macro-scale analysis was only conducted to verify the 3D model for bending assuming isotropic elastic properties. For viscoelastic analysis, viscoelastic input properties are needed. To define the viscoelastic behaviour of an isotropic material in Abaqus, an instantaneous elastic modulus is needed to represent the rate-independent elasticity of the material behaviour. The effective relaxation moduli are obtained by multiplying the instantaneous moduli with the dimensionless effective relaxation functions as given below (Section 22.7.1 in Abaqus Analysis User's Guide) [39].

$$G(t) = G_o\left[1 - \sum_{i=1}^{N} g_i\left(1 - exp\left(-\frac{t}{\tau_i}\right)\right)\right] \tag{5}$$

$$K(t) = K_o\left[1 - \sum_{i=1}^{N} k_i\left(1 - exp\left(-\frac{t}{\tau_i}\right)\right)\right] \tag{6}$$

where t is time, and G_o and K_o are the instantaneous glassy (unrelaxed) shear and bulk moduli determined from the instantaneous elastic moduli, E_o, and Poisson's ratio, υ_o

$$G_o = \frac{E_o}{2(1+\nu_o)} \tag{7}$$ $$K_o = \frac{E_o}{3(1-2\nu_o)} \tag{8}$$

The characteristic parameters of the Prony laws, g_i and k_i are the weight factors defined as:

$$g_i = \frac{G_i}{G_o} \tag{9}$$ $$k_i = \frac{K_i}{K_o} \tag{10}$$

where G_i and K_i are the shear and bulk moduli associated with the specific relaxation time (τ_i) and N is the number of Maxwell units.

For the viscoelastic analysis of an orthotropic composite, a user material subroutine (UMAT) based on the differential form (DF) of viscoelasticity is employed. It should be noted that the DF code is capable of modelling the viscoelastic behaviour of isotropic, transversely isotropic [35] and orthotropic [12] composite material in 3-D. Based on the DF of viscoelasticity, the relaxation functions $G(t)$ and $K(t)$ of an isotropic viscoelastic solid are defined individually in terms of a series of exponentials known as the Prony series:

$$G(t) = G_\infty + \sum_{i=1}^{N} G_i \, exp\,(\frac{-t}{\tau_i}) \quad (1) \qquad K(t) = K_\infty + \sum_{i=1}^{N} K_i \, exp\,(\frac{-t}{\tau_i}) \quad (2)$$

in which G_∞ and K_∞ represent the long-term shear and bulk moduli (relaxed), respectively. Comparing Eqs. (5-6) to Eqs. (11-12), the relaxed moduli can be described as:

$$G_\infty = G_o\left(1 - \sum_{i=1}^{N} g_i\right) \quad (3) \qquad K_\infty = K_o\left(1 - \sum_{i=1}^{N} k_i\right) \quad (4)$$

For orthotropic viscoelastic solids, the above equations can be generalized as described in [12] and [35] for each component of the stiffness matrix. The generalized formulations can be found in [38] and more details are provided in [12]. Using the generalized form of DF of viscoelasticity, the orthotropic behaviour of composite plates is investigated numerically at different loading rates and the results are compared with experimental data in Section 3.2.

3. Results and model validation

Due to the lack of experimental data for uncured woven composites at the micro- and meso-scale, it is difficult to determine the accuracy level of the modelling framework at smaller scales. Therefore, two separate analyses on elastic and viscoelastic materials are conducted based on available input parameters. First, the effective elastic properties of cured UD and woven composites are estimated and compared with the experimental data available in the literature. For this purpose, analytical micromechanics equations presented in [2, 12] are employed to estimate the mechanical elastic properties of the cured UD (AS4/8552) and 5HS woven (AS4/3501-6) thermoset composites. Results are compared with the experimental data provided in [40] and [2] for model validation at the micro- and meso-scale, respectively. For macro-scale model validation, the viscoelastic bending responses of woven prepregs composing 5HS fibres impregnated with an epoxy resin (Cycom 5320) are simulated separately based on limited experimental data for uncured woven composites; bending curves at different loading rates are compared with the experimental data reported in [23].

3.1. Elastic material

3.1.1. Micro-scale results

At the micro-scale, the effective elastic properties of the solid unidirectional circular fibre composites are predicted using the analytical micromechanics equations described in [12]. The properties of the constituent materials, i.e. the fibres and cured resin (listed in Table 2) are selected based on available experimental data for a specific fully cured composite (AS4/8552) in literature [40, 41]. The moduli of AS4/8552 were also predicted by Ersoy et al. [40] using an analytical approach based on the Self Consistent Field Micromechanics (SCFM) and Finite Element Based Micromechanics (FEBM) and presented in Table 3 for further comparisons. Additionally, the composite properties in its uncured form are examined using micromechanics equations [12]. The current predictions are compared to those of two conventional methods described in [40]. It should be noted that the elastic modulus of the uncured resin is assumed equal to 30 MPa (Table 2) as the authors [40] only mentioned that the elastic modulus before vitrification is generally rubber-like modulus of the order of a few MPa.

Table 3 demonstrates a good agreement between the present results for the cured composite and the experimentally measured values reported by Ersoy et al. [40]. Based on the assumption for missing data on uncured resin, the present calculations using the micromechanics equations [12] for the uncured composite are very close to the one predicted by FEBM [40]. Additionally, FEBM was found to be a better method than SCFM in predicting the composite elastic properties when the reinforcement and matrix moduli differ significantly. In other words, the micromechanics model described in [12] has been validated for predicting the effective elastic properties of cured UD circular fibre composites. However, the effective properties of uncured composites have not been determined experimentally by Ersoy et al. [40]. Hence, model validation at the micro-scale cannot be extended to uncured composites.

3.1.2. Meso-scale results

The effective elastic properties of the UD composites obtained from the micromechanics model can be used to estimate the effective elastic properties of the woven fabrics at the meso-scale considering the yarns' arrangement. As the overall stiffness of the cured woven composites are reported in the literature for certain yarns and resins (see Table 4), the meso-scale model can be validated separately from the micro-scale model and for a specific woven composite characterized thoroughly by Naik [2].

The meso-scale analysis involves discretely modelling the yarn architecture within a repeating unit cell (RUC) (see Fig.1). The woven composite is specified by known quantities such as filament diameter, yarn filament count, yarn packing density p_d, yarn spacing and overall fibre volume fraction. By assuming the same value of yarn architecture as described in [2], the unknown quantities such as yarn thickness, yarn cross-sectional areas, yarn crimp angle and yarn undulating paths which are required for a discrete yarn can be determined. Then, each yarn is discretized again into yarn slices. Finally, the three-dimensional effective properties are computed using the material properties (see Table 4), spatial orientation and volume fraction of each yarn slice in a volume averaging technique. The analytical procedure for the effective elastic properties of the RUC is implemented in MATLAB and results are compared with experimental data in Table 5. Table 5 also includes results obtained from 3-D finite element analysis and analytical technique using TEXCAD presented in [2]. It can be seen that the predicted elastic constants of 5-harness satin (5HS) weave composite agree well with data provided in [2].

3.2. Viscoelastic material

As described in the beginning of Section 3, there are gaps in the literature regarding the micro- and meso-scale characterisation of uncured woven composites. From an industry perspective, determining nine engineering constants for full characterization of orthotropic woven composites is extremely challenging. Hence, it is almost impossible to validate the accuracy of the modelling framework for estimating the properties of uncured composites at the smaller scales (i.e. micro- and meso-scale). Considering the importance of bending properties of uncured plies on wrinkle formation, the macro-scale simulation results are presented, and the viscoelastic modelling approach is validated separately based on available data on the bending behaviour of a specific woven composite loaded at different rates. A plate geometry with dimensions similar to the experiments of Alshahrani and Hojjati [23] is selected for this purpose (Fig. 4). The total length of the sample is 150 mm with an un-gripped length of 120 mm. The cross-sectional area of the sheet is 50 mm wide by 0.55 mm thick. Mesh type, and boundary conditions are similar to the bending verification model described in the previous section.

As the analysis of the bending behaviour during the composite forming process requires high curvature to accurately simulate the process, a tip displacement of 50 mm is applied (Fig. 5). It is also noted that the position of applied displacement is located 4 mm from the free end to avoid generating any tensile stresses on the sample during bending [23]. This distance is then excluded from the total length of the sample in bending moment calculations. As the deflection curve of the sheet has large slopes, the large deformation cannot be neglected in the expression of the curvature. Hence, the exact expression for curvature (Eq. 2) is used.

Prior to investigating the effect of loading rates on the time-dependent behaviour of uncured prepregs, the material is assumed to behave as an isotropic elastic solid. The material is then changed to orthotropic viscoelastic to represent the behaviour of textile composites. Unlike continuous materials such as sheet metal or cured solid composites, uncured textile sheets have a very low bending stiffness due to the possible relative movement of reinforcing fibres. According to [19], the plate theory relation between the tensile and the bending stiffness is no longer valid for uncured samples. In the previous work of the authors, Le et al. [38], the compressive stiffness of uncured prepregs was found to be mainly dominated by the resin modulus even in the presence of the fibres. The effect of fibres was found negligible on the compressive modulus of uncured composites due to their very small buckling load at the micro-scale. Therefore, for modelling purposes, the uncured composite plate in Fig. 2c is assumed to be composed of two different materials with two distinct moduli (E_t and E_c). The left-hand side of the plate is assumed to be under compression with E_c = 200 MPa while the right-hand side is under tension with E_t = 60 GPa based on literature data. The compressive modulus (E_c) has been estimated from the slope of stress-strain curve in the elastic region of the buckling test conducted by Alshahrani and Hojjati [26] (see Table 1). In the lack of experimental data on tensile properties of uncured composites, E_t is estimated to be 60 GPa based on a micro- and meso-scale analyses considering the fibre modulus of 200 GPa and yarn fibre volume fraction and overall volume fraction for the woven unit cell of 0.6 and 0.5 respectively. Knowing E_t, E_c, and the material cross-section, the position of the neutral axis (the *x*-axis) (see Fig. 2c) has been determined from the assumption that the resultant axial force acting on the cross-section is zero. This simple analysis enables us to estimate the effective bending stiffness of the uncured prepreg (E_{bend} or E_e) by converting the composite plate (E_c, E_t) into an equivalent plate made of only one material with E_e. The approach is known as the transformed-section method given by the following equation [36].

$$E_c I_c + E_t I_t = E_e I \tag{15}$$

in which I_c and I_t are the moments of inertia about the neutral axis (the *x*-axis) of the cross-sectional areas of two distinct materials, E_c and E_t respectively. I is the moment of inertia about the neutral axis of the homogeneous cross-section assumed with an effective bending modulus (E_e). Using Eq. (15), E_e becomes 700 MPa for an assumed homogeneous isotropic elastic cross-section. As perfect bonding has been assumed between the plies in this simple analysis, two more cases with E_t and E_c assigned to the entire plate sections are also considered to get the upper and lower bounds; only the lower bound is shown in Fig. 6 for clarity. Fig. 6 shows the lower bound of bending curve for the isotropic elastic plate with compressive modulus assumed for the entire cross-sections. The case with the effective bending modulus (E_e = 700 MPa) gives the same result as the case using biaxial elastic moduli for the cross-section under compression and tension during bending. Experimental data conducted by Alshahrani and Hojjati [23] for 5HS prepregs in warp direction are also presented in Fig. 6 for comparison purpose.

A mesh sensitivity analysis is also conducted in this study. The results have been summarized in Table 6. Similar results with maximum difference of ~1% in terms of deformed shape as well as the required force (F) to bend the laminate to tip displacement of 50 mm were noted. Based on the conducted convergence study, the 1.92 mm × 2 mm × 0.275 mm mesh (Mesh 2) was selected for subsequent cases.

As the anisotropic nature of woven composites may affect the deformation behaviours during forming [38], the orthotropic viscoelastic properties are considered in the bending behaviour. It should be emphasized, the fibre-bed, i.e. the slight waviness of the fibres in composites, has been considered to play an important role in carrying the load in the transverse direction at the early stage of cure [42]. Therefore, the fibre-bed elastic properties are incorporated into the micromechanics equations [12] at micro-scale to estimate the effective viscoelastic properties of the uncured UD prepreg before using such properties as input parameters for the meso-scale model [2]. The mechanical properties of the resin, fibre and fibre-bed that have been used for viscoelastic analysis at micro-scale are listed in Table 7 for composites assumed under compression (Table 7a), tension (Table 7b) and bending (Table 7c), respectively.

The fibre-bed properties are derived from the effective elastic properties of a dry prepreg estimated in [42]. Due to the lack of data on the properties of uncured resin [23], assumptions have been made in this research based on available data in the literature [43, 44]. The resin viscoelastic properties are kept unchanged to better understand the effect of fibre-bed on the bending response of composite plates and comparison purposes. Prony series constants for MTM45-1 [44] listed in Table 9 are assumed for validating the model against the experimental data reported in [23]. The fibre properties reported in [45] are used here, excluding the stiffness in the fibre direction. The longitudinal elastic modulus of the fibre and fibre-bed in compression (see Table 7a) are assumed to be equal to 80 MPa due to the very low buckling load of a single fibre demonstrated in [38]. Under tension, the same properties as in [45] (i.e. 210 GPa) (see Table 7b) are assumed. However, a low value for fibre Young's modulus is assumed (1.5 GPa, see Table 7c) following the review conducted in previous section (see Table 1) for uncured composites under bending. The effective viscoelastic properties of UD composites at micro-scale are determined by using analytical micromechanics equations following the approach presented in [12, 46]. It is noted that the fibre-bed elastic constants will be added to the resin relaxed modulus to obtain the modified resin properties which are later combined with fibre properties in the micromechanics equations. Table 8a, Table 8b and Table 8c demonstrate the predictions for UD composites under compression, tension and bending assumptions, respectively.

At meso-scale, the mechanical viscoelastic constants for 5-harness satin weave composites are predicted using the analytical model developed by Naik [2] and shown in Table 9. The analytical technique implemented in MATLAB is similar to the one described in the elastic section. A specific MATLAB script has been created for this purpose. Due to the missing data on the yarn architecture, most of the known quantities for a specified weave composite are taken from [2]. For example, Alshahrani and Hojjati [23] only provided information about the used prepreg such as the 6 k yarn size (k – one thousand filaments) and the thickness of the single uncured prepreg (0.55 mm). Inputs for constituents' properties such as resin and yarn properties of a RUC are taken from Table 7 and Table 8. The estimated mechanical properties of 5-harness satin weave composites provided in Table 9a, Table 9b and Table 9c correspond to the inputs from Table 8a, Table 8b and Table 8c, respectively.

It is worth mentioning that based on micro- and meso-scale analyses with the assumption of longitudinal fibre modulus (E_1) of 80 MPa (see Table 7a) and 210 GPa (see Table 7b) for uncured composites under compression and tension respectively, the in-plane properties of unrelaxed prepreg 5HS (E_{xx}) are estimated to be 190 MPa (see Table 9a) and 58 GPa (see Table 9b). Such values agree well with the predicted compressive modulus (E_c = 200 MPa) and tensile modulus (E_t = 60 GPa) of the isotropic elastic composite plate described earlier (see Section 3.2 and Fig. 6). A similar analysis using the transformed-section method (Eq. 15) may be applied to estimate the effective bending stiffness of the uncured prepreg. It is interesting that the computed value of 680 MPa matches the unrelaxed modulus of prepreg 5HS (see Table 9c) obtained from micro- and meso-scale analyses considering the longitudinal fibre modulus (E_1) of 1.5 GPa.

The differential approach for modelling the response of orthotropic viscoelastic structures developed by Malek et al. [46] requires the components of the relaxation matrix in addition to relaxed and unrelaxed engineering constants. These values could be defined by the Prony series expansions as given below:

$$E(t) = E^r + (E^u - E^r) \sum_{i=1}^{12} w_i \, e^{\left(-\frac{t}{\tau_i}\right)} \tag{5}$$

where E^r and E^u are the relaxed and unrelaxed Young's modulus, respectively. The assumed parameters w_i and τ_i are presented in Table 10. The unrelaxed and relaxed values and the Prony series parameters associated with each component are then obtained and given in Table 11 and Table 12 respectively.

Fig. 7 compares the orthotropic viscoelastic behaviours of 5HS prepregs made of different assumed values of fibre stiffness using UMAT with experimental data conducted by Alshahrani and Hojjati [23] in warp directions. It is noted that when the longitudinal fibre modulus is assumed to be 1.5 GPa, the bending behaviour of the composite plate agrees very well with the test data reported in [23]. It is interesting that the predicted uncured in-plane properties of the 5HS prepreg according to the assumed fibre stiffness of 1.5 GPa is 680 MPa (see Table 9c). This value is in a good correlation with the predicted parameter extracted from averaged relaxation curves conducted by Alshahrani and Hojjati [26] (see Table 1). Also, such effective bending stiffness can be computed from the in-plane properties of uncured prepreg under compression and tension using the transformed-method via Eq. (15), i.e. 190 MPa (see Table 9a) and 58 GPa (see Table 9b) for compressive and tensile moduli, respectively. Hence, the low value for the fibre bending stiffness should be attributed to the low compressive modulus of the uncured composites which is dominated by the resin viscoelastic properties for prepregs under bending. Moreover, such a low value of the longitudinal fibre modulus considered here (1.5 GPa) is consistent with previous findings in the literature (see Table 1). To better understand the effect of fibre modulus, another bending curve with the assumption of entire section having fibres with E_1 = 80 MPa (compression modulus) at micro-scale is added to Fig. 7.

To demonstrate the effect of loading rate on the bending behaviours of 5HS prepreg, macro-scale viscoelastic analysis using UMAT with three loading rates at 3 mm/sec, 6 mm/sec and 9 mm/sec as in the experiments conducted by Alshahrani and Hojjati [23] are also performed. The results are provided in Fig. 8. A similar trend in rate-dependent bending behaviour of both numerical simulations and experimental data can be observed; a higher loading rate results in the higher load required to bend the composite plates to the desired tip displacement of 50 mm.

4. Discussion

To emphasize the effect of ply anisotropy on the bending response of uncured/partially cured composites during forming, an isotropic viscoelastic case corresponding to the validation case discussed above (E_1 = 1.5 GPa, see Table 7c) is investigated using Abaqus built-in viscoelastic material model (IF). The initial properties for uncured or partially cured composites are the instantaneous Young's moduli, E_o, and Poisson's ratio, ν_o. The instantaneous Young's moduli is assumed as 680 MPa according to the uncured in-plane properties of 5HS composites presented in Table 9c. Poisson's ratio is kept unchanged and equal to 0.495. Viscoelastic properties are described using Prony series constants listed in Table 10. Experimental data conducted by Alshahrani and Hojjati [23] for 5HS prepregs in warp direction are also shown in Fig. 9 for comparison purpose. It can be observed that the higher transverse properties due to the presence of fibre and fibre-bed effect increase the required loads to reach the specific tip displacement.

To investigate the role of resin in viscoelastic bending behaviour, similar cases with the same material inputs for fibre stiffness but ignoring resin contribution in micro- and meso-scale analyses using micromechanics equations [2, 12] are considered. The material properties of UD and 5HS prepreg, as well as dry 5HS according to five selected input parameters of fibre stiffness in between 80 MPa to 2000 MPa are listed in Table 13 for consideration purpose. Fig. 10 compares bending moments in prepreg and dry 5 HS satin weave sample conducted by Alshahrani and Hojjati [23] and numerical analyses. Only two pairs of cases according to assumed fibre modulus of 1.5 GPa and 500 MPa (see Table 13) along with the experimental data are plotted in Fig. 10 for highlighting the contribution of resin to the bending results. It can be seen that the difference between prepreg and dry samples obtained from the experimental study [23] is higher than the one predicted by numerical analyses. However, it should be emphasized that the uncured resin properties have not been provided by Alshahrani and Hojjati [23] and therefore assumptions have been made in this study based on available data in the literature [43, 44]. The observed discrepancy in Fig. 10 may be attributed to the difference between the real rheological characteristics and the assumed values here. Assuming the fibre bending stiffness of 500 MPa, the bending behaviour of its dry 5HS composite correlates well with the corresponding experimental result.

5. Conclusion

An efficient multi-scale modelling approach was presented to predict the bending behaviour of viscoelastic composites under various loading rates. To improve simulation efficiency, analytical models were employed to estimate the effective mechanical properties of uncured/partially cured 5HS composites at micro- and meso-scales. For macro-scale simulations, a 3-D orthotropic material model implemented as a UMAT subroutine in Abaqus software was employed to implicitly account for the complex hierarchical nature of woven composites. Consequently, the proposed approach should be emphasized as a rapid method for determining the role of viscoelastic parameters and the yarns architecture on the out-of-plane bending behaviour essential for predicting wrinkle formation in woven composites.

A comprehensive literature search was conducted to obtain input properties for the model. While several researchers have explored the in-plane shear characteristics of woven composites, it was discovered that the in-plane Young's moduli of uncured UD and woven composites, as well as the viscoelastic shear properties of resins, have received little attention. Until now, studies have mostly focused on determining the in-plane shear properties of uncured composites to simulate the forming process. As demonstrated in this study, in addition to in-plane shear properties, the in-plane Young's moduli of composites in both tension and compression can significantly affect the out-of-plane response of thin composites. Hence, these properties should be thoroughly described to accurately predict wrinkle formation during composite manufacturing.

Due to scarcity of published data on the viscoelastic properties of uncured composites, assumptions were made in this paper for estimating the compression and tension properties of uncured woven composites using data from the literature. For the first time, the numerical results elucidated that the extremely low value for fibre longitudinal modulus commonly used in most other models is in fact an effective value that implicitly captures the combined effect of low compressive modulus and high tensile modulus of uncured composites in bending. Thus, additional experimental research on the viscoelastic characteristics of composites at the micro- and meso-scale is advised to better understand the formation of wrinkles caused by bending during cure.

A large body of research in the past has shown that the inter-ply slippage is one of the most important deformation mechanisms during the process of forming composites, particularly for multilayered textile prepregs. Therefore, the inter-ply slippage and its effect on the bending properties of thicker composites should be explored more rigorously in the future. Finally, it should be noted that the temperature effect was not considered in the paper. As the temperature is known to be an important parameter during forming, studying the variation of resin viscoelastic properties with temperature as well as inter-ply slippage and their effects on wrinkle formation (using the presented approach) are the subjects of our future work.

Acknowledgements

This research was supported by Vietnam International Education Cooperation Department – Ministry of Education and Training and University of Technology Sydney, Australlia.

Data Availibity

The raw/processed data required to reproduce these findings cannot be shared at this time due to technical or time limitations..

References

[1] Farnand K, Zobeiry N, Poursartip A, Fernlund G. Micro-level mechanisms of fiber waviness and wrinkling during hot drape forming of unidirectional prepreg composites. Composites Part A: Applied Science and Manufacturing. 2017;103:168-77.

[2] Naik RA. Analysis of woven and braided fabric reinforced composites. Washington DC: National Aeronautics and Space Administration; 1994.

[3] Hallander P, Sjölander J, Åkermo M. Forming induced wrinkling of composite laminates with mixed ply material properties; an experimental study. Composites Part A: Applied Science and Manufacturing. 2015;78:234-45.

[4] Margossian A, Bel S, Hinterhoelzl R. Bending characterisation of a molten unidirectional carbon fibre reinforced thermoplastic composite using a Dynamic Mechanical Analysis system. Composites Part A: Applied Science and Manufacturing. 2015;77:154-63.

[5] Long AC. Design and manufacture of textile composites. Cambridge: Woodhead Publishing Limited, 2005.

[6] Alshahrani H, Hojjati M. Bending behavior of multilayered textile composite prepregs: Experiment and finite element modeling. Materials & Design. 2017;124:211-24.

[7] Belnoue JPH, Hallett SR. A rapid multi-scale design tool for the prediction of wrinkle defect formation in composite components. Materials & Design. 2020;187.

[8] Dewangan MK, Panigrahi SK. Multi-scale modeling of three-dimensional angle interlock woven composite subjected to ballistic impact using FEM. Polymers for Advanced Technologies. 2020;31:3079-94.

[9] Dewangan MK, Panigrahi SK. Multiscale modelling of 3D orthogonal woven composite under ballistic impact using FEM. Fibers and Polymers. 2020;21:2389-400.

[10] Dewangan MK, Panigrahi SK. Factors influencing the ballistic impact mechanisms of textile composite materials: a review. Polymers for Advanced Technologies. 2021;32:1901-23.

[11] Matouš K, Geers MGD, Kouznetsova VG, Gillman A. A review of predictive nonlinear theories for multiscale modeling of heterogeneous materials. Journal of Computational Physics. 2017;330:192-220.

[12] Malek S. Efficient multi-scale modelling of viscoelastic composites with different microstructures [PhD Thesis]. Canada: University of British Colombia, 2014.

[13] Alshahrani H. Characterization and finite element modeling of coupled properties during polymer composites forming processes. Mechanics of Materials. 2020;144.

[14] Larberg Y, Åkermo M. In-plane deformation of multi-layered unidirectional thermoset prepreg – Modelling and experimental verification. Composites Part A: Applied Science and Manufacturing. 2014;56:203-12.

[15] Haanappel SP, ten Thije RHW, Sachs U, Rietman B, Akkerman R. Formability analyses of uni-directional and textile reinforced thermoplastics. Composites Part A: Applied Science and Manufacturing. 2014;56:80-92.

[16] Boisse P, Colmars J, Hamila N, Naouar N, Steer Q. Bending and wrinkling of composite fiber preforms and prepregs. A review and new developments in the draping simulations. Composites Part B: Engineering. 2018;141:234-49.

[17] Liang B, Hamila N, Peillon M, Boisse P. Analysis of thermoplastic prepreg bending stiffness during manufacturing and of its influence on wrinkling simulations. Composites Part A: Applied Science and Manufacturing. 2014;67:111-22.

[18] Belnoue JPH, Nixon-Pearson OJ, Thompson AJ, Ivanov DS, Potter KD, Hallett SR. Consolidation-Driven Defect Generation in Thick Composite Parts. Journal of Manufacturing Science and Engineering. 2018;140.

[19] Boisse P, Hamila N, Vidal-Salle E, Dumont F. Simulation of wrinkling during textile composite reinforcement forming. Influence of tensile, in-plane shear and bending stiffnesses. Composites Science and Technology. 2011;71:683-92.

[20] Martin TA, Bhattacharyya D, Collins IF. Bending of fibre-reinforced thermoplastic sheets. Composites Manufacturing. 1995;6:177-87.

[21] Bilbao E, Soulat D, Hivet G, Gasser A. Experimental Study of Bending Behaviour of Reinforcements. Experimental Mechanics. 2009;50:333-51.

[22] Wang J, Long AC, Clifford MJ. Experimental measurement and predictive modelling of bending behaviour for viscous unidirectional composite materials. International Journal of Material Forming. 2009;3:1253-66.

[23] Alshahrani H, Hojjati M. A new test method for the characterization of the bending behavior of textile prepregs. Composites Part A: Applied Science and Manufacturing. 2017;97:128-40.

[24] Skordos AA, Monroy Aceves C, Sutcliffe MPF. A simplified rate dependent model of forming and wrinkling of pre-impregnated woven composites. Composites Part A: Applied Science and Manufacturing. 2007;38:1318-30.

[25] Haanappel SP, Akkerman R. Shear characterisation of uni-directional fibre reinforced thermoplastic melts by means of torsion. Composites Part A: Applied Science and Manufacturing. 2014;56:8-26.

[26] Alshahrani H, Hojjati M. A theoretical model with experimental verification for bending stiffness of thermosetting prepreg during forming process. Composite Structures. 2017;166:136-45.

[27] Hallander P, Akermo M, Mattei C, Petersson M, Nyman T. An experimental study of mechanisms behind wrinkle development during forming of composite laminates. Composites Part A: Applied Science and Manufacturing. 2013;50:54-64.

[28] Sjölander J, Hallander P, Åkermo M. Forming induced wrinkling of composite laminates: A numerical study on wrinkling mechanisms. Composites Part A: Applied Science and Manufacturing. 2016;81:41-51.

[29] Dörr D, Schirmaier FJ, Henning F, Kärger L. A viscoelastic approach for modeling bending behavior in finite element forming simulation of continuously fiber reinforced composites. Composites Part A: Applied Science and Manufacturing. 2017;94:113-23.

[30] Alshahrani H. Bending behaviour of textile thermosetting composite prepregs during forming processes. Montreal, Canada: Concordia University, 2017.

[31] Dangora LM, Mitchell CJ, Sherwood JA. Predictive model for the detection of out-of-plane defects formed during textile-composite manufacture. Composites Part A: Applied Science and Manufacturing. 2015;78:102-12.

[32] Yu WR, Zampaloni M, Pourboghrat F, Chung K, Kang TJ. Analysis of flexible bending behavior of woven preform using non-orthogonal constitutive equation. Composites Part A: Applied Science and Manufacturing. 2005;36:839-50.

[33] Dangora LM, Mitchell C, White KD, Sherwood JA, Parker JC. Characterization of temperature-dependent tensile and flexural rigidities of a cross-ply thermoplastic lamina with implementation into a forming model. International Journal of Material Forming. 2016;11:43-52.

[34] DSM. HB80 product specification sheet. 26-02-2014 ed. US2014. p. 1/.

[35] Zobeiry N, Malek S, Vaziri R, Poursartip A. A differential approach to finite element modelling of isotropic and transversely isotropic viscoelastic materials. Mechanics of Materials. 2016;97:76-91.

[36] Gere J, M,., Goodno BJ. Mechanics of material: Global Engineering, 2009.

[37] Timoshenko S. Strength of materials. United States of America1940.

[38] Le VA, Zobeiry N, Erkmen E, Malek S. Buckling behaviour of laminated viscoelastic composites under axial loads. Mechanics of Materials. 2021.

[39] Abaqus I. Abaqus Analysis User's Guide. USA: Dassault Systèmes Simulia Corp.; 2013.

[40] Ersoy N, Garstka T, Potter K, Wisnom MR, Porter D, Clegg M, et al. Development of the properties of a carbon fibre reinforced thermosetting composite through cure. Composites Part A: Applied Science and Manufacturing. 2010;41:401-9.

[41] Zobeiry N, Forghani A, Li C, Gordnian K, Thorpe R, Vaziri R, et al. Multiscale characterization and representation of composite materials during processing. Philos Trans A Math Phys Eng Sci. 2016;374:20150278.

[42] Malek S, Vaziri R, Poursartip A. Application of a generalised cellular solid model for predicting the fibre-bed effective properties in viscoelastic modelling of fibre reinforced composites. 18th European Conference on Composite Materials. Athens, Greece2018.

[43] Niaki SA, Forghani A, Vaziri R, Poursartip A. A three-phase integrated flow-stress model for processing of composites. Mechanics of Materials. 2018;117:152-64.

[44] Thorpe R. Experimental characterization of the viscoelastic behavior of a curing epoxy matrix composite from pre-gelation to full cure. Canada: University of British Colombia, 2012.

[45] Johnston A, Vaziri R, Poursartip A. A plane strain model for process-induced deformation of laminated composite structures. Journal of Composite Materials. 2001;35:1435-69.

[46] Malek S, Gereke T, Zobeiry N, Vaziri R. Multi-scale modelling of time-dependent response of composite structures made of orthotropic viscoelastic materials. 13th International Conference on Steel, Space and Composite Structures. Perth, Australia2018.

Figures

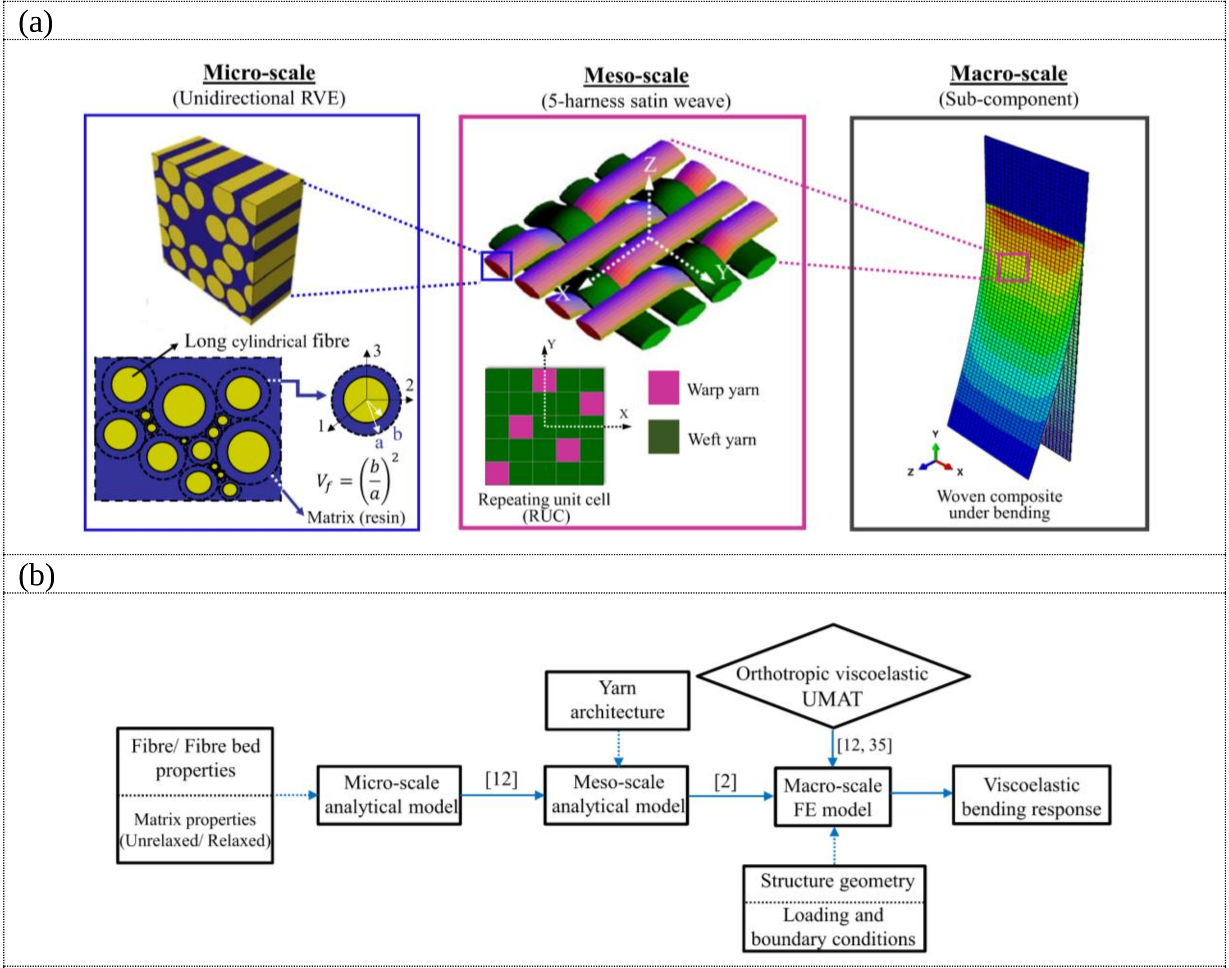

Figure 1: (a) Schematic of the multi-scale modelling approach for bending behaviour of 5-harness satin weave composites from micro-scale to macro-scale; (b) Flow chart depicting the analytical and numerical models utilized in the multi-scale analysis.

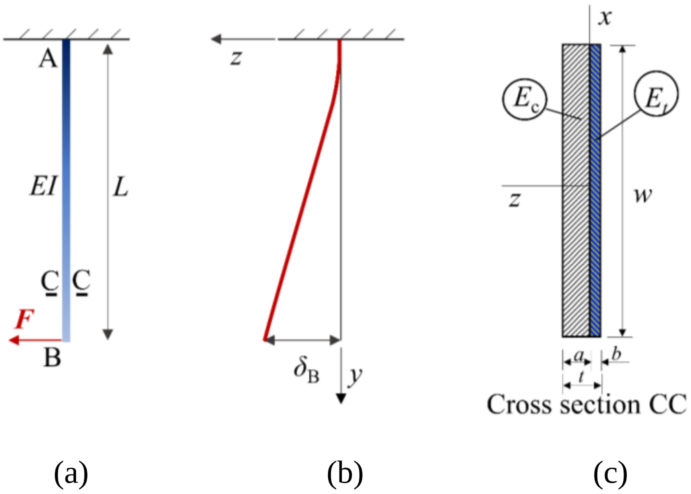

Figure 2: Bending of a cantilever beam based on the test conducted in [23]: (a) beam with load; (b) deflection curve; (c) cross-section of beam showing the x-axis as the neutral axis of the cross-section.

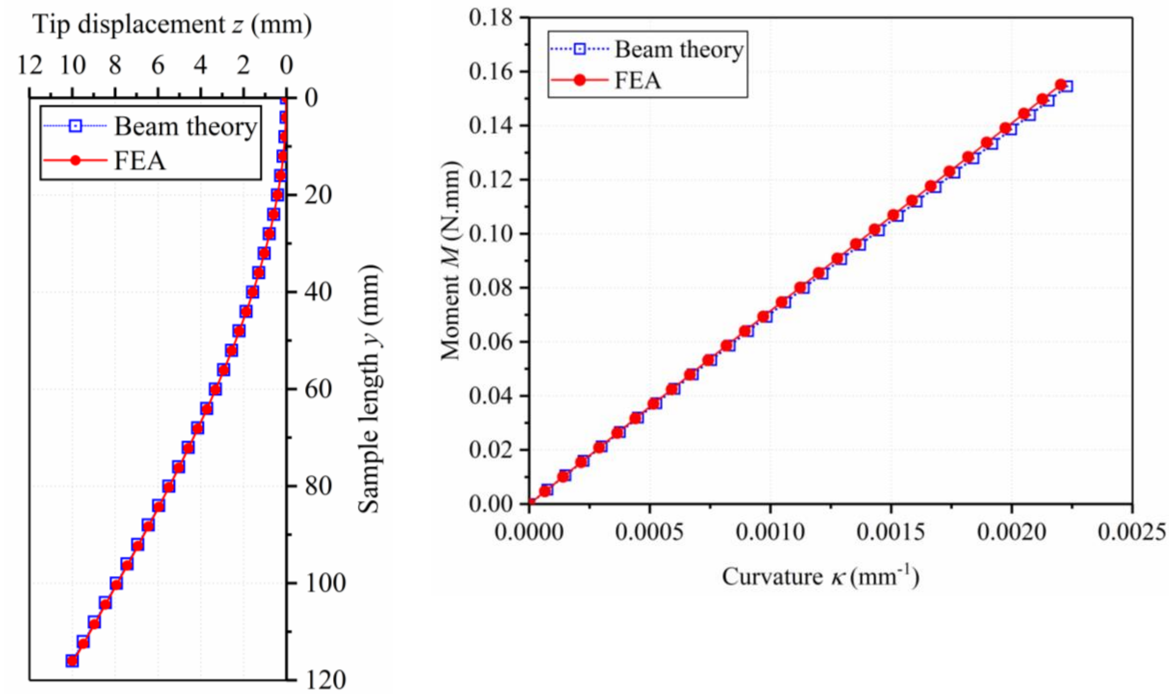

(a) (b)

Figure 3: (a) Bending profile with tip displacement of 10 mm
(b) Bending moment – curvature relation in the isotropic elastic beam (E = 500 MPa, υ = 0.2)

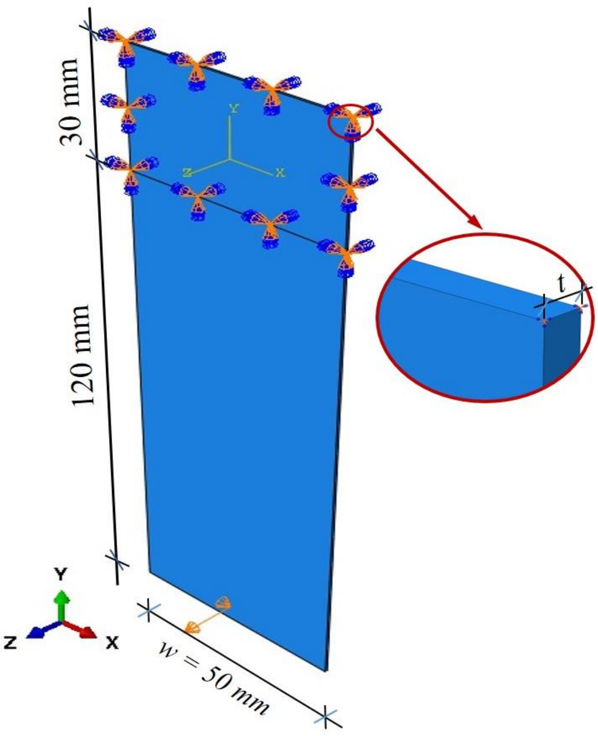

Figure 4: Detail of the 3D model under bending
(According to [23])

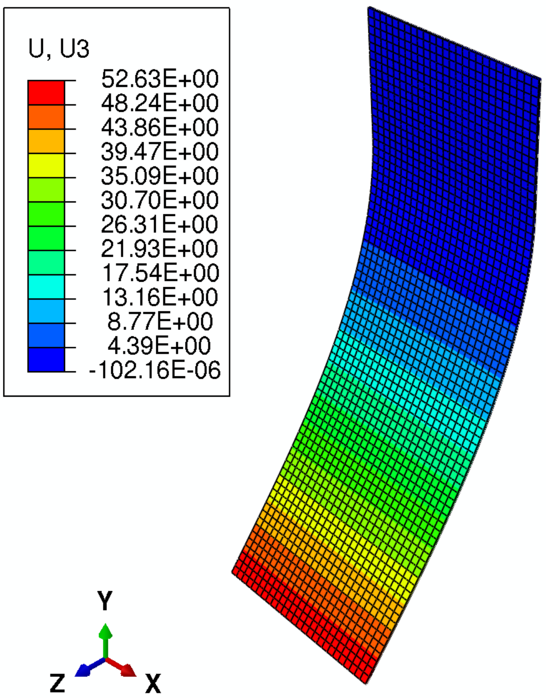

Figure 5: Deformed sample at tip displacement of 50 mm (U_3 in mm)

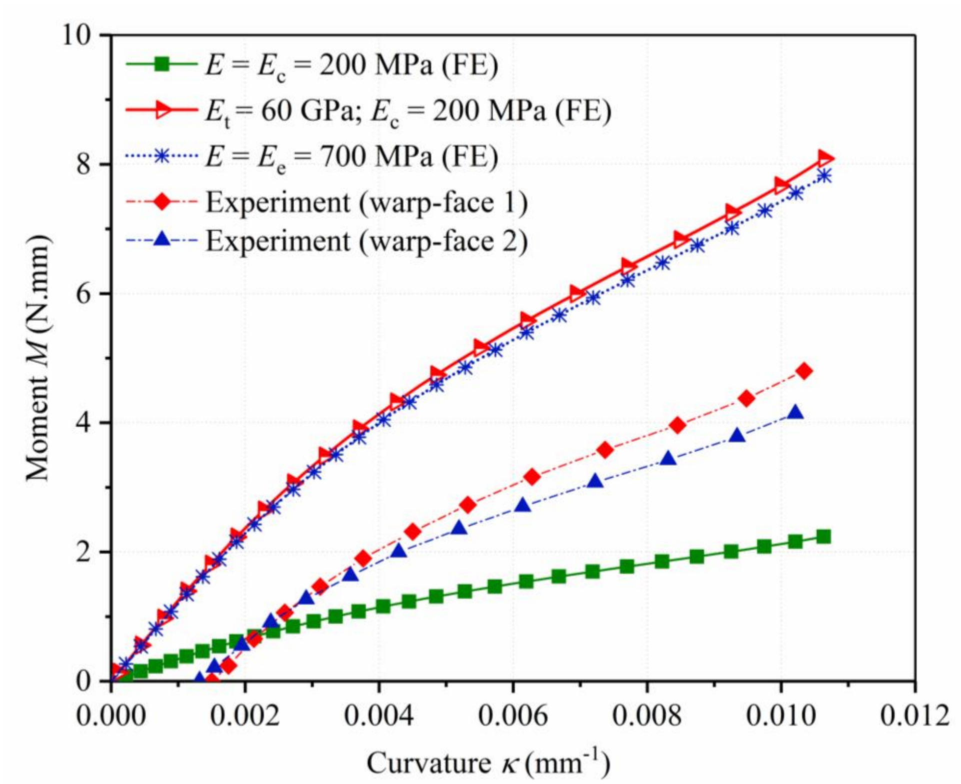

Figure 6: Bending moment versus curvature based on isotropic elastic material assumption.

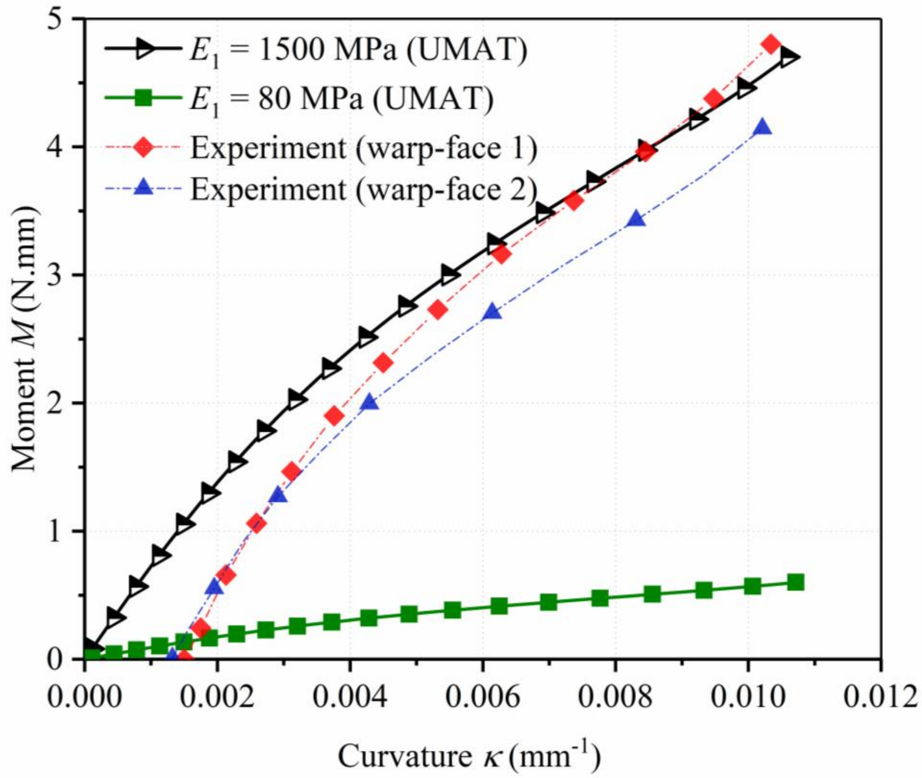

Figure 7: Bending moment versus curvature of uncured 5HS prepreg with different values of fibre stiffness (E_1). A loading rate of 3 mm/s is considered for all cases.

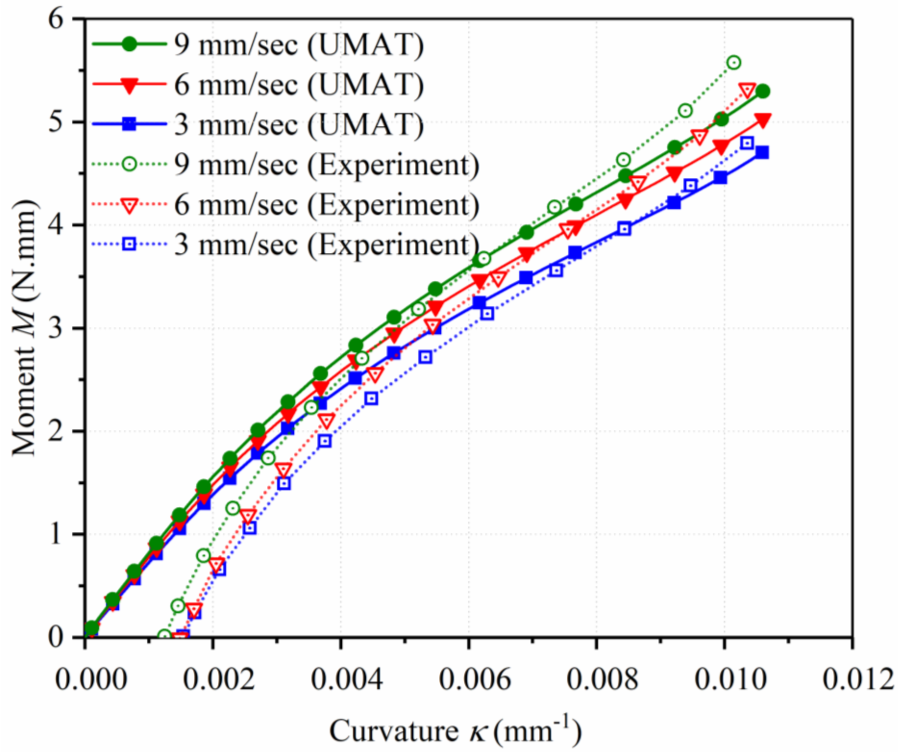

Figure 8: Effect of loading rate on bending moment versus curvature of 5HS prepreg. Fibre stiffness is assumed to be E_1 = 1.5 GPa in all cases.

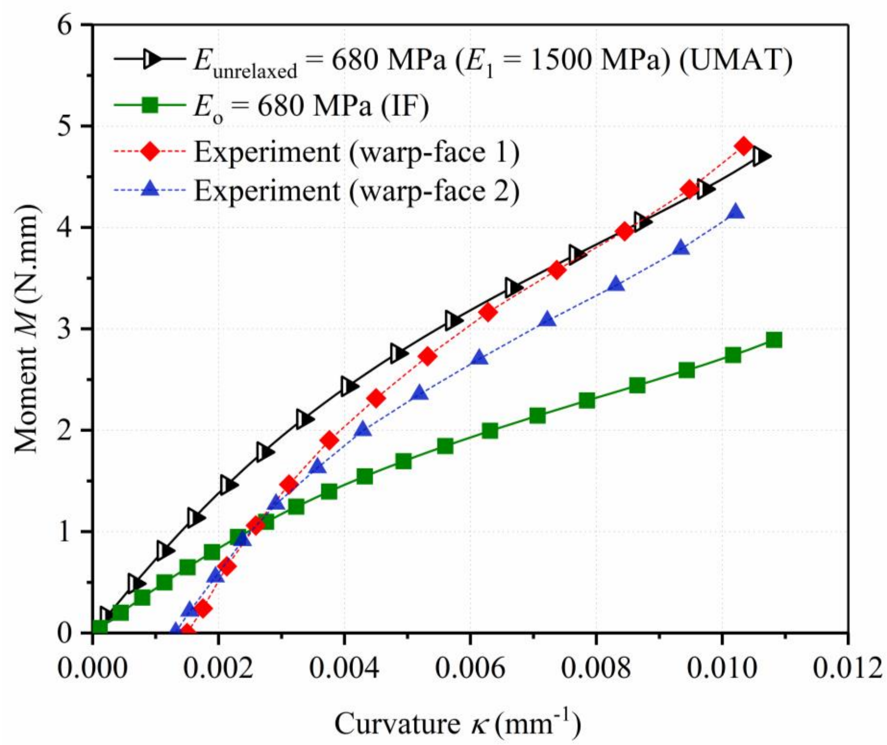

Figure 9: Comparison between IF and DF approaches for the validation case (effective fibre modulus E_1 = 1.5 GPa). The viscoelastic properties of the resin are provided in Table 10.

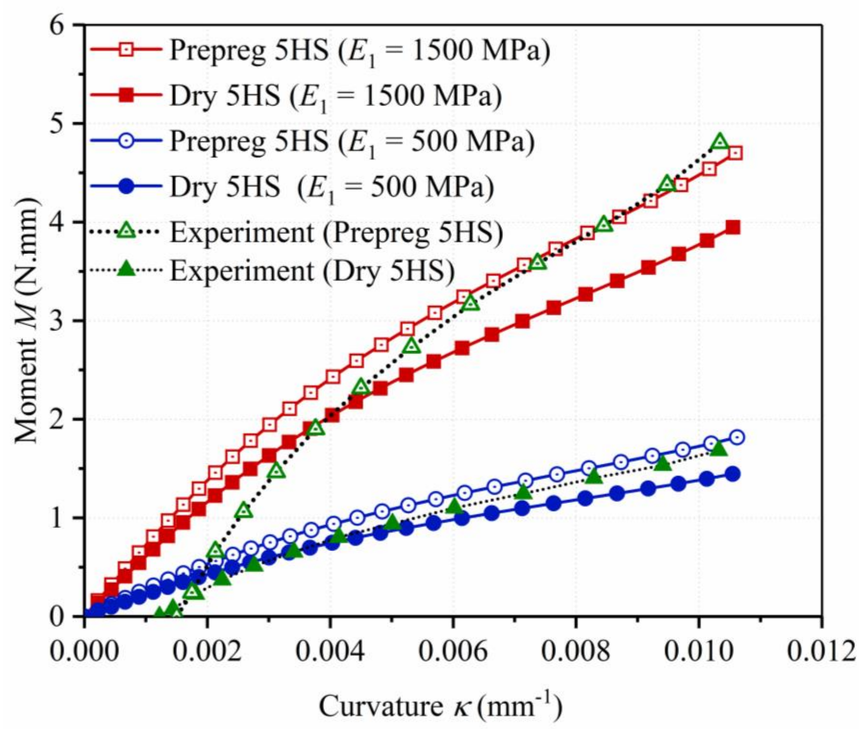

Figure 10: Comparison between prepreg and dry 5HS behaviour according to different assumed values for fibre bending stiffness, E_1.

Tables

Table 1: List of experimental studies on deformation of uncured composites and calibrated material properties for the corresponding FE simulations.

Fibre modulus (E_1) in MPa	Material	Test	Temperature	Loading rate	Reference
1000	Cross-plied UD thermoset prepregs	Bias extension		40 mm/min	[14]
	T700/M21		85°C		
	HTS/977-2		70°C		
1000	Glass 8HS/PPS	Bias extension	310°C	25, 100, 400 mm/min	[15]
1000 for HT fibres and 1200 for IM fibres	Stacked UD prepreg with the same epoxy matrix and - HT carbon fibres - IM carbon fibres	Bias extension	70°C	0.05 mm/min	[28]
100[a]		Bending			
1000	5HS satin weave (6 k carbon fibre tows with Cycom 5320)	Bias extension	70°C	20 mm/min	[6]
275[b]		Bending			
1200	5HS satin weave (6 k carbon fibre tows with Cycom 5320)	Bias extension	Room temperature	20 mm/min	[13]
580[b]		Bending			
125[b]	PA6-CF UD-Tape	Rheometer bending	260°C		[29]
735 – 40000[c]	IMA-M21	Bending	110°C - 30°C		[18]
14000 – 44000[d]	Dyneema HB80	Tensile	120°C - 20°C	102 mm/min	[33]
0.015[e]	Glass/PP commingled plain weave	Bending			[32]
150 – 200[f] for weft/warp	5HS satin weave (6 k carbon fibre tows with Cycom 5320)	Buckling	Room temperature	180 mm/min	[26]
600 – 700[g] for weft/warp		Bending	70°C		

[a] Bending stiffness in the fibre direction used in the orthotropic elastic model for out-of-plane properties.
[b] Isotropic Hooke modulus represents an elastic spring in the viscoelastic material model for the out-of-plane bending elements.
[c] Young's modulus of the prepreg sheet in the fibre direction against temperature.
[d] Tensile modulus of Dyneema HB80 in the fibre direction against temperature.
[e] Asymmetric factor.
[f] Compressive modulus of the prepreg samples.
[g] Unrelaxed modulus of the prepreg samples under bending at forming conditions.

Table 2: Constituent's elastic properties of cured and uncured UD thermoset composite according to [40].

V_f = 0.574

Property	Unit	Fibre	Resin (8552)	
		AS4	Uncured*	Cured
E_1	GPa	228	0.03	4.67
$E_2 = E_3$	GPa	17.20		
$G_{12} = G_{13}$	GPa	27.60	0.010	1.70
G_{23}	GPa	5.73		
$v_{12} = v_{13}$	-	0.2	0.499	0.37
v_{23}	-	0.5		

Notes*: For uncured resin, Young's modulus is assumed to equal to 30 MPa as the authors only mentioned that the elastic modulus before vitrification is generally rubber-like modulus of the order of a few MPa.

Table 3: Comparison of the UD composite elastic properties obtained by the present analysis [12] and data available in the literature [40].

Property	Unit	SCFM		FEBM		Measured	Present	
		Uncured	Cured	Uncured	Cured	Cured	Uncured	Cured
E_{11}	MPa	131,000	133,000	132,200	134,000	135,000	130,890	133,100
$E_{22} = E_{33}$	MPa	122	9,130	165	9,480	9,500	146.2	9,626
$G_{12} = G_{13}$	MPa	41.1	5,210	44.3	5,490	4,900	36.94	5,202
G_{23}	MPa	37.2	3,210	41.6	3,272	4,900	36.71	3,139
$v_{12} = v_{13}$	-	0.327	0.272	0.346	0.271	0.300	0.327	0.267
v_{23}	-	0.639	0.465	0.982	0.448	0.450	0.991	0.534

Notes: The 1-axis is along the fibre direction, the 2-axis is perpendicular to the fibres but in the plane of the lamina and the 3-axis is the out-of-plane direction.
SCFM: Self Consistent Field Micromechanics [40].
FEBM: Finite Element Based Micromechanics [40].
Measured: Supplied by AIRBUS UK except for G_{23}; G_{23} is measured by Ersoy et al. [40] (no data for uncured state).
Present: Based on micromechanical equations in [12].

Table 4: Yarn and resin properties used in validation model for woven composite properties according to [2].

Material	E_{11} GPa	$E_{22} = E_{33}$ GPa	G_{12} GPa	ν_{12}	ν_{23}
Yarn	144.8	11.73	5.52	0.23	0.3
Resin	3.45	3.45	1.28	0.35	0.35

Table 5: Comparison of results for cured woven composites according to different methods.

Laminate type	Method	E_{xx}, E_{yy} GPa	E_{zz} GPa	G_{xz}, G_{yz} GPa	G_{xy} GPa	ν_{xz}, ν_{yz}	ν_{xy}
5-harness satin weave (5HS)	TEXCAD[a]	66.33	11.51	4.93	4.89	0.342	0.034
	FEM[a]	65.99	11.38	5.03	4.96	0.320	0.030
	Test[a]	69.43	-	-	5.24	-	0.060
	Present	65.45	11.77	4.73	4.89	0.337	0.035

Notes: [a] presented in [2]
xy-plane is the plane of woven fabric

Table 6: Convergence study results (isotropic elastic case (E = 700 MPa, ν = 0.4)).

	Mesh 1	Mesh 2	Mesh 3	Mesh 4
Num. of Elements	2,401	3,901	8,209	16,417
Num. of Nodes	13,846	22,264	46,350	80,086
Force F (N)	6.754×10^{-02}	6.751×10^{-02}	6.746×10^{-02}	6.736×10^{-02}
Simulation time (sec)	167	285	655	1867

Coarse mesh
Fine mesh

Mesh: Num in X × num in Y × num in Z (see XYZ coordinate in Fig. 4)
Mesh 1: 20 × 60 × 2 Mesh 3: 36 × 114 × 2
Mesh 2: 26 × 72 × 2 Mesh 4: 36 × 114 × 4

Table 7a: Input material properties of fibre, resin and fibre bed used in the bending simulation of textile prepregs. The compressive properties have been assigned to the bending model.

V_f = 0.600

Property	Unit	Fibre[1]	Resin[2]		Fibre bed[3]
			Relaxed	Unrelaxed	
E_1	GPa	8.00×10^{-2}	3.00×10^{-6}	1.65×10^{-1}	8.00×10^{-2}
$E_2 = E_3$	GPa	1.72×10^{-1}	3.00×10^{-6}	1.65×10^{-1}	1.12×10^{-4}
$G_{12} = G_{13}$	GPa	27.60	1.00×10^{-6}	5.52×10^{-2}	1.13×10^{-4}
G_{23}	GPa	0.07	1.00×10^{-6}	5.52×10^{-2}	4.49×10^{-5}
$v_{12} = v_{13}$	-	0.2	0.495	0.495	
v_{23}	-	0.25	0.495	0.495	0.250

Notes: [1] Taken from [45] except E_1, E_2 (compressive moduli); compressive moduli, E_1, E_2 are selected according to [38]
[2] Resin properties are taken from [43]
[3] Taken from [42] except E_1 (compressive modulus); compressive modulus, E_1, is selected according to [38]

Table 7b: Input material properties of fibre, resin and fibre bed used in the bending simulation of textile prepregs. The tensile properties have been assigned to the bending model.

V_f = 0.600

Property	Unit	Fibre[1]	Resin[2]		Fibre bed[3]
			Relaxed	Unrelaxed	
E_1	GPa	2.10×10^{2}	3.00×10^{-6}	1.65×10^{-1}	2.10×10^{2}
$E_2 = E_3$	GPa	1.72×10^{1}	3.00×10^{-6}	1.65×10^{-1}	1.12×10^{-4}
$G_{12} = G_{13}$	GPa	27.60	1.00×10^{-6}	5.52×10^{-2}	1.13×10^{-4}
G_{23}	GPa	6.88	1.00×10^{-6}	5.52×10^{-2}	4.49×10^{-5}
$v_{12} = v_{13}$	-	0.2	0.495	0.495	
v_{23}	-	0.25	0.495	0.495	0.250

Notes: [1] Taken from [45]
[2] Resin properties are taken from [43]
[3] Taken from [42]

Table 7c: Input material properties of fibre, resin and fibre bed used in the bending simulation of textile prepregs. The effective bending properties have been assigned to the model.

V_f = 0.600

Property	Unit	Fibre[1]	Resin[2] Relaxed	Resin[2] Unrelaxed	Fibre bed[3]
E_1	GPa	1.50×10^{0}	3.00×10^{-6}	1.65×10^{-1}	1.50×10^{0}
$E_2 = E_3$	GPa	1.72×10^{-1}	3.00×10^{-6}	1.65×10^{-1}	1.12×10^{-4}
$G_{12} = G_{13}$	GPa	27.60	1.00×10^{-6}	5.52×10^{-2}	1.13×10^{-4}
G_{23}	GPa	0.07	1.00×10^{-6}	5.52×10^{-2}	4.49×10^{-5}
$v_{12} = v_{13}$	-	0.2	0.495	0.495	
v_{23}	-	0.25	0.495	0.495	0.250

Notes:[1] Taken from [45] except E_1, E_2; E_1, E_2 are selected following the comprehensive review in the literature (see Table 1)
[2] Resin properties are taken from [43]
[3] Taken from [42] except E_1; E_1 is selected following the comprehensive review in the literature (see Table 1)

773

Table 8a: Micro-scale predictions of UD mechanical properties using micromechanics equations with fibre-bed effect [12] under compressive load.

Properties of UD	Unit	Present Relaxed	Present Unrelaxed
E_{11}	MPa	64.03	110.8
$E_{22} = E_{33}$	MPa	1.689	169.1
$G_{12} = G_{13}$	MPa	0.456	219.6
G_{23}	MPa	0.443	63.02
$v_{12} = v_{13}$	-	0.316	0.340
v_{23}	-	0.905	0.341

774

Table 8b: Micro-scale predictions of UD mechanical properties using micromechanics equations with fibre-bed effect [12] under tensile load.

Properties of UD	Unit	Present	
		Relaxed	Unrelaxed
E_{11}	GPa	168.0	168.0
$E_{22} = E_{33}$	MPa	1.707	830.5
$G_{12} = G_{13}$	MPa	0.456	219.6
G_{23}	MPa	0.446	213.2
$v_{12} = v_{13}$	-	0.316	0.318
v_{23}	-	0.913	0.947

Table 8c: Micro-scale predictions of UD mechanical properties using micromechanics equations with fibre-bed effect [12] under bending load.

Properties of UD	Unit	Present	
		Relaxed	Unrelaxed
E_{11}	MPa	1.200	1.246
$E_{22} = E_{33}$	MPa	1.693	193.2
$G_{12} = G_{13}$	MPa	0.456	219.6
G_{23}	MPa	0.443	63.02
$v_{12} = v_{13}$	-	0.316	0.346
v_{23}	-	0.909	0.523

Table 9a: Meso-scale predictions of 5HS prepreg mechanical properties under compression using the analytical technique of Naik [2].

Laminate type	Material	E_{xx}, E_{yy} MPa	E_{zz} MPa	G_{xz}, G_{yz} MPa	G_{xy} MPa	v_{xz}, v_{yz}	v_{xy}
5HS	Relaxed resin	24.10	5.80	7.08×10^{-1}	3.79×10^{-1}	0.798	0.002
	Unrelaxed resin	190.70	248.90	118.60	187.10	0.360	0.578

Table 9b: Meso-scale predictions of 5HS prepreg mechanical properties under tension using the analytical technique of Naik [2].

Laminate type	Material	E_{xx}, E_{yy} GPa	E_{zz} GPa	G_{xz}, G_{yz} GPa	G_{xy} GPa	ν_{xz}, ν_{yz}	ν_{xy}
5HS	Relaxed resin	57.26	0.02	0.039	3.80×10^{-4}	0.870	1.68×10^{-4}
	Unrelaxed resin	58.94	6.66	1.055	0.192	0.849	0.003

Table 9c: Meso-scale predictions of 5HS prepreg mechanical properties under bending using the analytical technique of Naik [2].

Laminate type	Material	E_{xx}, E_{yy} MPa	E_{zz} MPa	G_{xz}, G_{yz} MPa	G_{xy} MPa	ν_{xz}, ν_{yz}	ν_{xy}
5HS	Relaxed resin	412.60	8.40	5.10	3.80×10^{-1}	0.800	2.94×10^{-4}
	Unrelaxed resin	680.20	394.10	126.20	187.20	0.676	0.212

Table 10: Prony series parameters for MTM45-1 epoxy as reported in [44].

Maxwell Element (*i*)	w_i	τ_i (s)
1	0.344181	1×10^{-2}
2	0.114728	1×10^{-1}
3	0.133849	1×10^{0}
4	0.152970	1×10^{1}
5	0.133849	1×10^{2}
6	0.095606	1×10^{3}
7	0.019121	1×10^{4}
8	0.003824	1×10^{5}
9	0.001338	1×10^{6}
10	0.000382	1×10^{7}
11	0.000096	1×10^{8}
12	0.000038	1×10^{9}

Table 11: Unrelaxed and relaxed values of components of the composite relaxation matrix. The effective bending properties have been assigned to the model at micro-scale.

Component	C_{ij}^{r}(MPa)	C_{ij}^{u}(MPa)
C_{11}	629.6	1757.2
C_{22}	629.6	1757.2
C_{33}	17.6	1212.3
C_{44}	0.8	375.0
C_{55}	19.7	258.2
C_{66}	19.7	258.2
C_{12}	5.0	1039.8
C_{13}	25.1	1041.7
C_{23}	25.1	1041.7

781

Table 12: Prony series parameters for each component of the relaxation matrix of the composite material obtained from micromechanics equations following the approach presented in [46]. The effective bending properties have been assigned to the model at micro-scale.

i	w_{11}	w_{22}	w_{33}	w_{44}	w_{55}	w_{66}	w_{12}	w_{13}	w_{23}
1	388.098	388.098	411.193	128.793	82.087	82.087	356.158	349.894	349.894
2	129.367	129.367	137.066	42.931	27.363	27.363	118.721	116.632	116.632
3	150.928	150.928	159.909	50.086	31.923	31.923	138.507	136.071	136.071
4	172.489	172.489	182.753	57.241	36.483	36.483	158.293	155.509	155.509
5	150.928	150.928	159.909	50.086	31.923	31.923	138.507	136.071	136.071
6	107.805	107.805	114.220	35.776	22.802	22.802	98.933	97.193	97.193
7	21.561	21.561	22.844	7.155	4.560	4.560	19.786	19.438	19.438
8	4.312	4.312	4.569	1.431	0.912	0.912	3.957	3.887	3.887
9	1.509	1.509	1.599	0.501	0.319	0.319	1.385	1.360	1.360
10	0.431	0.431	0.456	0.143	0.091	0.091	0.395	0.388	0.388
11	0.108	0.108	0.114	0.036	0.023	0.023	0.099	0.097	0.097
12	0.043	0.043	0.046	0.014	0.009	0.009	0.040	0.039	0.039

782

Table 13: Summary of composite properties for UD and 5HS prepregs, as well as dry UD and 5HS according to different values of fibre stiffness, E_1.

Fibre E_1 (MPa)	Prepreg				Dry	
	E_{11} (MPa) (UD)		E_{xx}, E_{yy} (MPa) (5HS)		E_{11} (UD) (MPa)	E_{xx}, E_{yy} 5HS (MPa)
	Relaxed	Unrelaxed	Relaxed	Unrelaxed		
2,000	1,600.00	1,645.10	549.10	836.10	1,600.00	549.10
1,500	1,200.00	1,246.00	412.60	680.20	1,200.00	412.60
1,000	800.03	846.30	276.10	519.00	800.03	276.10
500	400.03	446.34	139.50	348.10	400.03	139.50
80	64.03	110.76	24.10	190.70	64.03	24.10